

# Atomistic Origins of Ductility Enhancement in Metal Oxide Coated Silicon Nanowires for Li-Ion Battery Anodes

Anthony Gao, Sankha Mukherjee, Ijya Srivastava, Matthew Daly, and Chandra Veer Singh\*

Silicon nanowires (SiNWs) are a promising anode material for Li-ion batteries due to their exceptionally high charge capacity. However, direct implementation is hindered by large volume expansion induced during lithiation, which results in mechanical failure during repeated charge cycling. Recent experimental works show thin metal oxide coatings can significantly increase the cycle stability of SiNWs. However, the deformation mechanisms underpinning this performance enhancement are not understood, presenting an opportunity for a fundamental investigation of core–shell mechanics. In this study, molecular dynamics simulations investigating the mechanical behavior of silica- and alumina-coated SiNWs under uniaxial tension are performed. Metal oxide coated nanowires possess significantly improved ductility, increasing the elongation to failure from 16% to greater than 47%. This occurs without significant reduction in tensile strength, resulting in apparent toughness 2–4 times that of uncoated nanowires. During loading, the oxide coating absorbs strain energy through breaking of bonds between highly coordinated atoms. At the same time, the coating maintains the structural integrity of the silicon core by increasing the defect nucleation rate from the core-coating interface, preventing localized deformation. Under both athermal (0 K) and room temperature conditions, the underlying deformation mechanism changes from amorphization within a localized shear band to dislocation twinning and large-scale amorphization.

capacity ( $\approx 3500 \text{ mAh g}^{-1}$ ), low voltage hysteresis, low operating potential ( $\approx 0.4 \text{ V vs Li/Li}^+$ ), and the relatively high abundance and low cost of lithium.<sup>[5,6]</sup> However, one of the major roadblocks in the commercialization of silicon-based electrodes is their poor mechanical performance when used in a rechargeable battery. When fully charged, the Si anode in a LIB can undergo a volume expansion of up to 400% which causes stress concentrations, resulting in premature chemomechanical failure of the anode. Consequently, the active components of the battery lose electronic contact causing poor cycle life and reduced capacity. In this regard, SiNWs below a critical size (below 150 nm in diameter) have been reported to accommodate this high strain without fracture owing to their increased strain relaxation, increased flaw tolerance, and reduced Li-ion diffusion paths.<sup>[7,8]</sup> However, this large surface area to volume ratio also presents a large surface for solid electrolyte interphase (SEI) layer formation. Repeated breaking and reformation of this SEI layer due to volume expansion during cycling leads to irreversible consumption

of Li ions, which in turn causes poor Coulombic efficiency and reduced life.<sup>[9,10]</sup>

Experimental results have shown that while uncoated SiNWs are only capable of sustaining  $\approx 10$  charge–discharge cycles before irreversible loss in lithiation charge capacity, the addition of coatings on SiNWs, such as carbon,<sup>[11]</sup> polymers,<sup>[12]</sup> and metal oxides<sup>[13,14]</sup> can enhance the battery stability to between 50 and 100 cycles. This improvement is clearly visible even at nanometer thicknesses, making thin-film deposition processes such as atomic layer deposition (ALD) attractive techniques for performance enhancement.<sup>[15]</sup> First, thin oxide coatings ( $\text{Al}_2\text{O}_3$ ,  $\text{SiO}_2$ ,  $\text{TiO}_2$ , etc.) are capable of functioning as an artificial SEI, inhibiting solid electrolyte interphase film formation and activity across the nanowire surface due to their insulating and high dielectric properties.<sup>[16,17]</sup> This inhibits the formation of  $\text{Li}_2\text{CO}_3$  and  $\text{LiF}$ , and other organic SEI components, preventing irreversible consumption of Li-ions during cycling.<sup>[18]</sup> Additionally, the addition of thin coatings has also been found to improve the mechanical integrity of the silicon core itself by constraining volume expansion and reducing

## 1. Introduction

In recent years, silicon nanowires (SiNWs) have attracted increased attention due to their unique size-dependent properties. These make them attractive for use in a number of applications, including nanoelectronics,<sup>[1]</sup> nanosensors,<sup>[2]</sup> catalysis,<sup>[3]</sup> and Li-ion battery (LIB) anodes.<sup>[4]</sup> In many cases, these applications depend on the strong mechanical behavior of the nanowires (NWs) for them to function reliably. For example, Si is a potential candidate to replace traditional graphite-based anodes used in Li-ion batteries, owing to factors such as their high theoretical charge

A. Gao, Dr. S. Mukherjee, I. Srivastava, Dr. M. Daly, Prof. C. V. Singh  
Department of Materials Science and Engineering  
University of Toronto  
Toronto, ON M5S 3E4, Canada  
E-mail: chandraveer.singh@utoronto.ca

 The ORCID identification number(s) for the author(s) of this article can be found under <https://doi.org/10.1002/admi.201700920>.

DOI: 10.1002/admi.201700920

stress concentration.<sup>[19]</sup> Experimental works have shown that SiNWs coated with metal oxide coatings, such as alumina or titania, have fewer cracks than uncoated SiNWs after cycling.<sup>[20]</sup> Recently, Kim et al.<sup>[19]</sup> have performed molecular dynamics (MD) simulations to track the chemical, structural evolution of Al<sub>2</sub>O<sub>3</sub> coatings during lithiation, wherein it has been reported that concentration gradients of Li-ions are formed inside the oxide coating, resulting in elastic modulus gradient and delayed failure.<sup>[21]</sup> However, it is still not clear to what extent oxide coatings improve the mechanical properties of the SiNWs or to what extent the ultimate tensile strength (UTS), Young's modulus, ductility, and toughness improve as a function of oxide coating thickness. Optimization of parameters, such as coating thickness and core diameter, is required to develop an artificial SEI coating which can withstand the volume expansion of silicon during multiple lithiation cycles.

In this study, the effects of silica and alumina coatings on the mechanical properties of SiNWs are examined using molecular dynamics simulations with a reactive force field (ReaxFF).<sup>[22,23]</sup> From a mechanics perspective, it is known that while properties such as the Young's modulus of core-shell nanowires follow typical mixing rules, other properties can show unexpected phenomena. For instance, the core-shell interface of crystalline-amorphous silicon nanowires has been found to provide a site for surface defect nucleation, decreasing the tensile strength and increasing ductility.<sup>[24]</sup> Additionally, the failure mechanisms of core-shell nanowires appear to be profoundly influenced by the interaction of the constituent materials. For example, Si-coated AuNWs can sustain a plastic deformation of up to 50% strain without undergoing necking due to the ability of the silicon coating to prevent localized deformation.<sup>[25]</sup> Motivated by these findings, this study intends to evaluate the potential ability for ALD coatings to provide mechanical integrity to SiNW battery anodes. To this end, we have performed uniaxial tensile tests on both coated and uncoated SiNWs, at

both 0 and 300 K. A parametric study is performed, considering the effects of SiNW core diameter, coating thickness, and operating temperature. The effect of coating thickness on UTS and strain to failure will help to optimize coating design, and varying the SiNW diameter will help to determine how results might apply to larger SiNWs. Simulations with nanowires composed entirely of either silica or alumina are also performed to determine if the properties of coated nanowires follow traditional mixing rules. Finally, insight is given into the deformation and failure mechanisms of both uncoated and coated SiNWs, at both 0 and 300 K.

## 2. Computational Modeling

The MD simulations were carried out using LAMMPS software<sup>[26]</sup> with a ReaxFF potential.<sup>[22,23]</sup> This ReaxFF potential designed for Li, Al, Si, and O is part of a series of variable charge bond-order potentials in which the total energy of the system is described by bonding including, Coulombic, overcoordination, and van der Waals energies. ReaxFF potentials have previously been used in simulations of other SiNW systems, including those with lithiation of both bulk silicon and SiNWs.<sup>[19,27–29]</sup> The total simulation cell measured 10.3 nm × 15.0 nm × 15.0 nm, with the atmosphere around the SiNWs being vacuum (**Figure 1**). All the nanowires tested had an initial length of 10.3 nm, with periodic boundary conditions in all the orthogonal directions; the loading direction was oriented along the <111> crystallographic direction of the NW. All MD simulations were performed using the canonical (NVT) during tensile loading and the isothermal-isobaric (NPT) ensemble for equilibration, with temperature controlled using a Nosé–Hoover thermostat and a damping parameter of 100 fs.<sup>[30]</sup> A timestep of 1 fs was used. Visualization of nanowire deformation was achieved using The Open Visualization Tool (OVITO).<sup>[31,32]</sup>

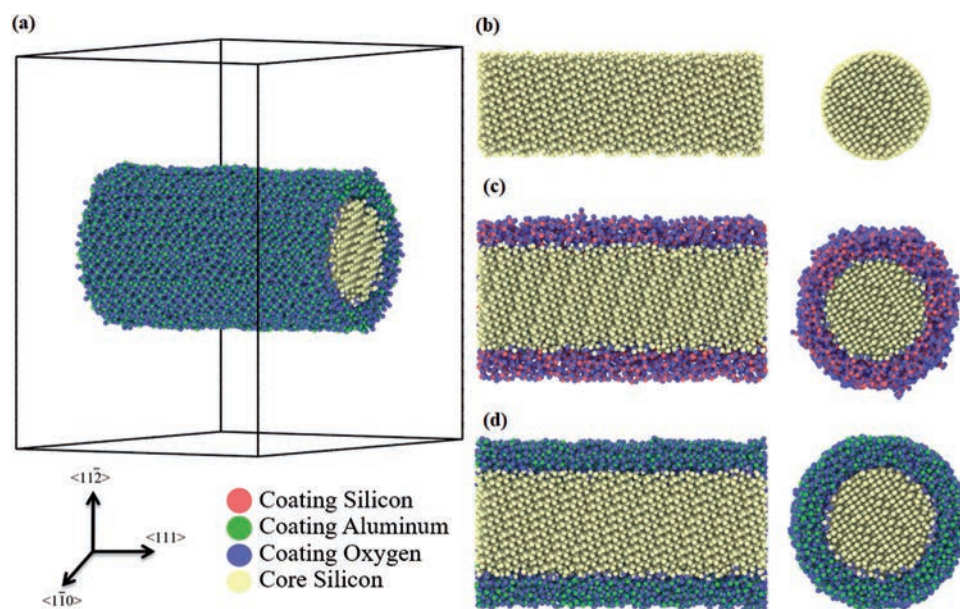


**Figure 1.** Snapshots showing a schematic illustration of a) the simulation cell containing an alumina-coated nanowire, with horizontal and vertical cross-sections of 4 nm diameter SiNW: b) uncoated, c) with 1.0 nm silica coating, and d) 1.0 nm alumina coating.

Crystalline SiNWs are first relaxed at 0 and 300 K, before loading in the axial direction until failure at a strain rate of  $0.1\% \text{ ps}^{-1}$ . Uniaxial tensile loading is achieved through incremental dilations of the simulation supercell. Atomic positions are then rescaled through a commensurate affine transformation, which effectively creates a uniaxial strain equal to the box dilation. Atoms were permitted to statically relax after each dilation step; however, the strained box dimension was held constant. For studying the overall stress–strain response, the longitudinal stress  $\sigma_{xx}$  was calculated using the component of the pressure tensor in the direction of strain  $p_{xx}$ , with the initial diameter of the nanowire used to calculate the characteristic volume, and time averaged over 1 ps. It should be noted that at 300 K for the ReaxFF potential, thermal equilibration of the uncoated SiNWs results in surface reconstruction causing distortion in the diamond cubic lattice structure, similar to what is obtained using the Tersoff potential.<sup>[33]</sup> Following annealing at high temperature to remove dislocations, the resulting structure is still recognizable as diamond cubic by the modified common neighbor analysis, described by Maras et al.<sup>[34]</sup> SiNWs at 0 K remained fully diamond cubic without any annealing required. Silica or alumina coatings are added after annealing according to their most stable bulk configuration and relaxed to an amorphous structure prior to testing. Simulations with nanowires composed entirely of either silica or alumina are also performed to determine if the properties of coated nanowires follow traditional mixing rules. A full list of nanowire parameters tested can be seen in the Supporting information.

### 3. Results and Discussion

#### 3.1. Deformational Behavior of Uncoated SiNWs

In order to establish a reference for comparison, the tensile responses of uncoated SiNWs are presented first. **Figure 2** shows the tensile response of uncoated SiNWs with diameters ranging from 2 to 6 nm. At 300 K, the nanowires are initially crystalline with reconstructed surfaces. The uncoated SiNWs with diameters greater than 4 nm exhibit linear elastic loading with Young's moduli between 132 and 142 GPa up to a strain of 5% and a stress of 6 GPa, after which localized surface amorphization begins to occur. This corresponds to a noticeable decline in the slope of the stress–strain curve, although continued loading causes it to rise again as amorphous region is seen to extend beyond the coating into the SiNW core, resulting into the formation of a shear band (Figure 2a). This leads to failure as necking occurs at the UTS of  $\approx 11$  GPa at 16% strain. These values are relatively consistent with the recent experimental measurements of Zhang et al., which report a UTS of 18 GPa at 13.5% strain with Young's modulus of 134 GPa<sup>[35]</sup> for SiNWs, as well as other MD simulations.<sup>[36]</sup> It should be noted that although our value of 11 GPa is low compared to experimental results, increasing nanowire diameter has been reported to correlate with an increase in UTS.<sup>[37]</sup> Although the strain to failure also increases with increasing diameter, beyond a size of 4 nm the marginal gains are limited. In addition, we find that the effect of diameter size on Young's modulus is not significant. These results for the UTS and elastic modulus demonstrate the geometric dependence of

mechanical properties of SiNWs at 300 K, which is also consistent with other MD simulations.<sup>[36,38]</sup>

At 0 K, the uncoated SiNWs exhibit linear loading behavior up until a peak stress, followed by a sharp drop in the stress state after continued loading. For the uncoated SiNW this is at about 10% strain, with UTSs and an elastic modulus of 14.4 and 163 GPa. These values are in agreement with other MD simulations.<sup>[39,40]</sup> The SiNW fails via amorphization upon reaching the peak stress. After a period of prolonged necking, during which some hardening is observed to occur (as per the stress-strain response in Figure 2b), fracture ultimately occurs. It is difficult to verify this counterintuitive hardening profile, as we are operating in a very nonlaboratory regime in terms of thermal effects. Additionally, it can be observed that at 0 K, the Young's modulus, UTS, and strain to UTS are comparable for all the SiNWs irrespective of their diameter. This is similar to the results of Liu and Shen,<sup>[41]</sup> which also find negligible effects of size on mechanical properties of SiNWs at low temperature.

Although the failure mechanisms for SiNWs have been studied before using atomistic simulations, our simulations reveal interesting insights on aspects that have previously remained unclear. For instance, different interatomic potentials often show varying results for UTS, elongation to failure, and failure mechanisms.<sup>[37]</sup> Kang et al. showed whether a potential predicts a brittle or ductile failure mechanisms depends on the value of a ductility parameter consisting of the Schmid factor  $S$  multiplied by the ratio between the ideal tensile and shear strengths ( $S\sigma_c/\tau_c$ ), which suggests that for the SiNWs considered here cleavage should occur, because SiNWs are stronger in shear than in tension.<sup>[36]</sup> A subsequent investigation indicated that ductility also depends on nanowire diameter, temperature, and strain rate, with a brittle to ductile transition when the nanowire diameter falls below 4 nm at room temperature.<sup>[37]</sup>

However, for all nanowire diameters tested here, failure does not occur via crack propagation but via shear-driven amorphization within a dominant shear band. This finding is in agreement with recent experimental studies such as by Han et al.,<sup>[42]</sup> who showed that  $\langle 111 \rangle$  oriented crystalline SiNWs turn into amorphous Si during tensile loading via shear-driven mechanism in which an intermediate diamond–hexagonal phase is formed followed by dislocation nucleation and accumulation.<sup>[43]</sup> This crystalline to ductile transition has also been recently observed in compression of silicon pillars via accumulation of stacking faults.<sup>[44]</sup>

To illustrate the atomistic mechanism based on our Reax-based simulations, a sequence of atomic configurations during various stages of tensile deformation between nanowires with diameters of 4 and 6 nm is depicted in Figure 2a. The smaller diameter nanowires fail by tensile necking, while the larger nanowires fail following the development of localized shear bands. For all sizes tested, amorphization originates from the surface and propagates through the nanowire core. At 0 K, a failure continues to occur via amorphization, which initiates from the surface and penetrates through the core. While failure at 300 K typically results with the formation of a single shear band, multiple shear bands were observed to form throughout the entire nanowire volume at 0 K. These shear bands accumulated to form a large tensile neck in all the samples tested. To understand whether the deformation close to failure occurs via phase transformation, we counted the number of atoms belonging to the regions that underwent phase

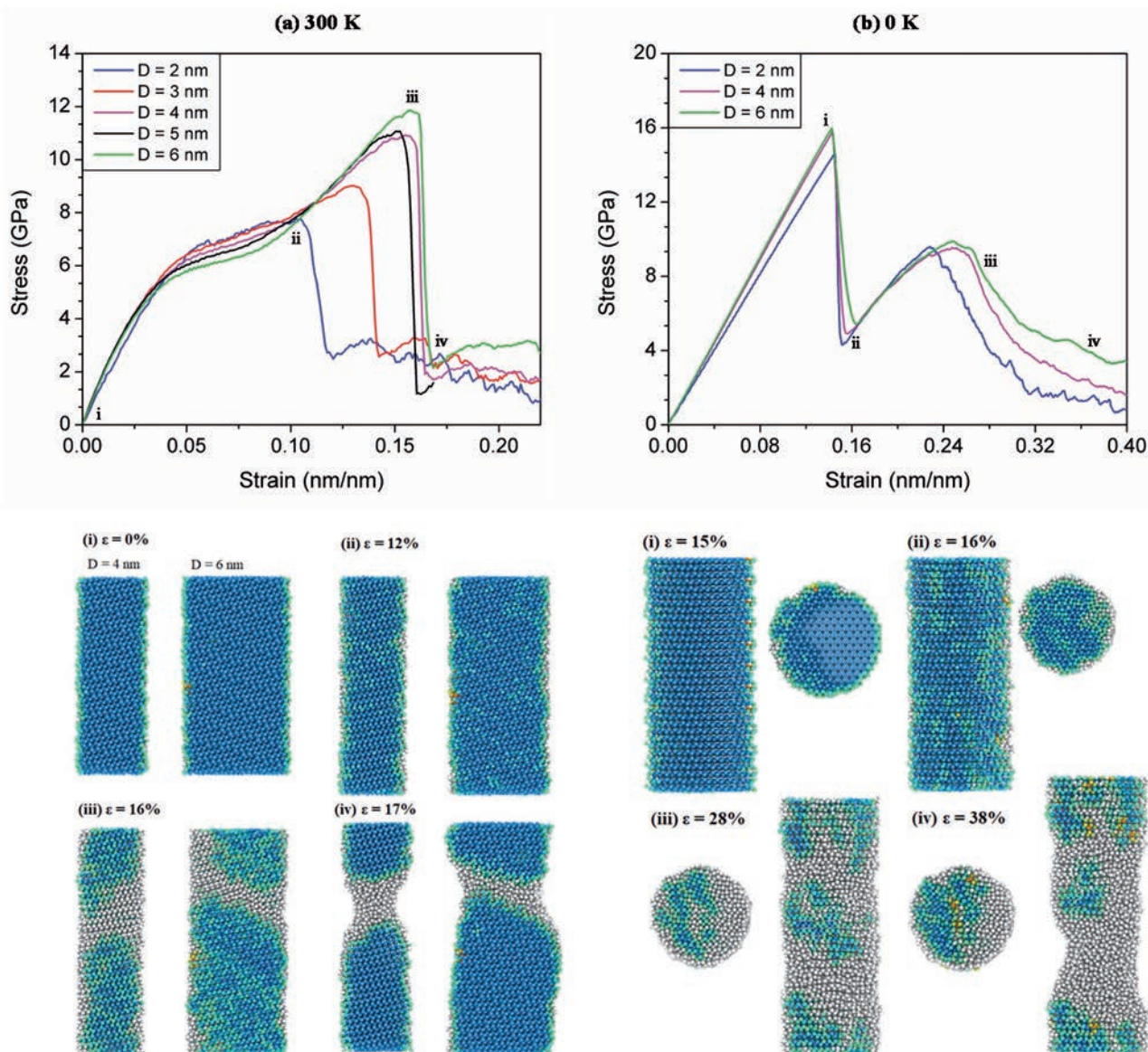


**Figure 2.** Stress–strain curves for uncoated SiNWs undergoing tension with a strain rate of  $0.1\text{ ps}^{-1}$  at both at a) 300 and b) 0 K, with snapshots showing the underlying failure mechanisms below. Atoms are colored according to the modified centrosymmetry by Maras et al.<sup>[34]</sup> to identify diamond cubic structure. Atoms in blue are diamond cubic; orange are diamond hex. Lighter shades indicate 1st and 2nd neighbors of crystalline phases, while white atoms are not recognized as belonging to any crystal structure. a) The cross sections of two nanowires of diameter of 4 and 6 nm at 300 K are pictured. By 16% strain a shear band forms, leading to localized failure. b) A nanowire with diameter of 6 nm is presented. Multiple shear bands form during deformation, although failure still occurs via plastic flow within a dominant shear band.

change to nondiamond cubic lattice using a modified centrosymmetry parameter.<sup>[34]</sup> For a nanowire with diameter of 6 nm, at 300 K only 18% of atoms were detected as nondiamond cubic close to failure initiation, while greater than 67% of atoms were observed as nondiamond cubic at 0 K. Here, failure is defined as the point when the stress falls below 35% of the UTS.

### 3.2. Deformational Behavior of Metal Oxide Coated SiNWs

**Figure 3** compares the stress–strain curves of SiNWs of diameter  $D = 4.0$  nm with 0.5, 1.0, and 1.5 nm silica and alumina

coatings at 300 K and a strain rate of  $0.1\text{ ps}^{-1}$ . All cases of silica coatings resulted in ductile deformation with delayed failure and improved toughness in comparison to uncoated NWs. The overall elongation to failure appears to be limited primarily by the strain at which failure initiates in the silica coating, which occurs at 40–47% strain. During the tensile simulation, atomic readjustment occurs intermittently, corresponding to sharp drops in the stress–strain curves that are clearly visible in the stress–strain responses. The overall change in mechanical properties due to the coating on nanowire properties appears to be dependent on the thickness of the coating. For all silica-coated nanowires tested, the UTS decreases to  $\approx 9$  GPa, but

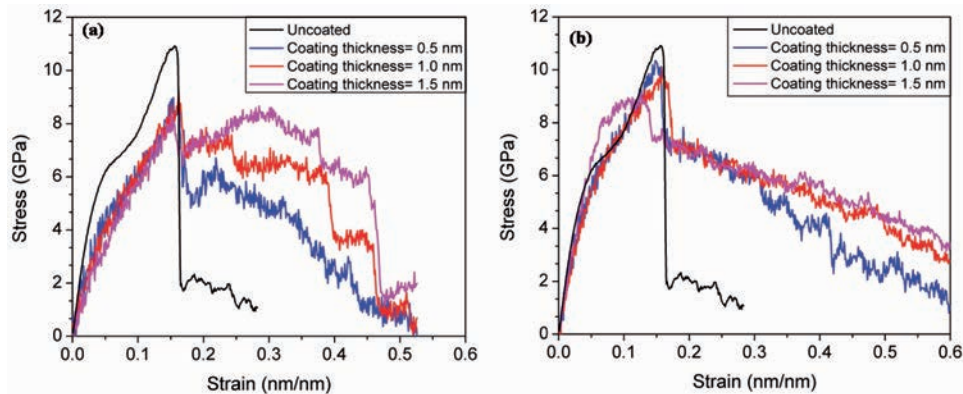


**Figure 3.** The effect of coating thickness (0.5, 1.0, and 1.5 nm) is shown in the stress–strain curves for SiNWs with a) silica and b) alumina coatings, with strain rate  $0.1\% \text{ ps}^{-1}$  at 300 K and a core diameter of 4 nm.

at 16% strain (failure of uncoated SiNWs), a drop in stress of  $\approx 3$  GPa occurs for the 0.5 thick coating, while coating thicknesses of 1.5 and 1 nm result in a drop of only  $\approx 1$  GPa. As the ratio of coating thickness to nanowire diameter decreases, a higher stress drop is expected, since the UTS of silica is not reached until failure at roughly 40–47% strain (**Figure 4**). This allows the silica coating to provide a relatively stiff outer layer which absorbs further load. However, for Li-ion battery anodes, this may not be preferable, since a highly stiff coating imposes compressive constraints on the Si core, inhibiting lithiation.<sup>[19,45]</sup>

For the case of alumina coatings also, significant improvements in elongation to failure and toughness were observed. However, in contrast to silica-coated NWs, these improvements were found to be relatively size independent in the case of alumina coatings and the gains for coating thickness beyond 1.0 nm appear to be marginal (**Figure 3b**). All coated nanowires displayed similar Young's moduli and the UTS measurements appear to decrease slightly as coating thickness increased. Following the onset of yielding, the stress plateaued at  $\approx 7$  GPa and slowly reduced as necking occurred. As coating thickness increased, both the final elongation to failure and the energy absorbed up to failure improved diminishingly, and to a lesser extent than silica coatings. In addition, higher thickness also resulted in reduced UTS, indicating that thicker coatings are not necessarily mechanically superior. This property

makes thin alumina coatings such as provided by ALD ideal for mechanical property enhancement in applications such as Li-ion battery anodes, where diffusion of lithium ions is slowed in oxide coatings as the formation of Li–O bonds presents a barrier to lithium diffusion.<sup>[27]</sup>

Since silicon nanostructures used in Li-ion batteries and other applications typically have core diameters on the order of 50–150 nm,<sup>[8]</sup> it is necessary to determine how changing diameter sizes may affect our results. **Figure 4** shows the effect of oxide coatings on the mechanical properties of SiNWs with different core diameters (2 and 6 nm, respectively). For both alumina and silica coatings, the UTS increases with core diameter due to the improved properties of the Si core. As such, it is expected that as the Si core diameter increases, the UTS of our coated nanowires should continue to increase to up to  $\approx 20$  GPa.<sup>[35]</sup> However, beyond 16% strain, when failure of uncoated SiNWs occurs, the ability of the coating to improve performance decreases with increasing core diameter. This is especially noticeable for silica coatings, where an SiNW with core diameter of 2 nm has a strain to failure of 70%, but only 38% at 6 nm. This corresponds to experimental results which have shown that while a 3.4 nm thick silica coating can inhibit volume expansion in SiNWs with diameter of  $\approx 50$  nm, an SiNW with a diameter of 150 nm requires a  $\approx 7$  nm thick coating to achieve a similar effect.<sup>[46,47]</sup> Alumina coatings have

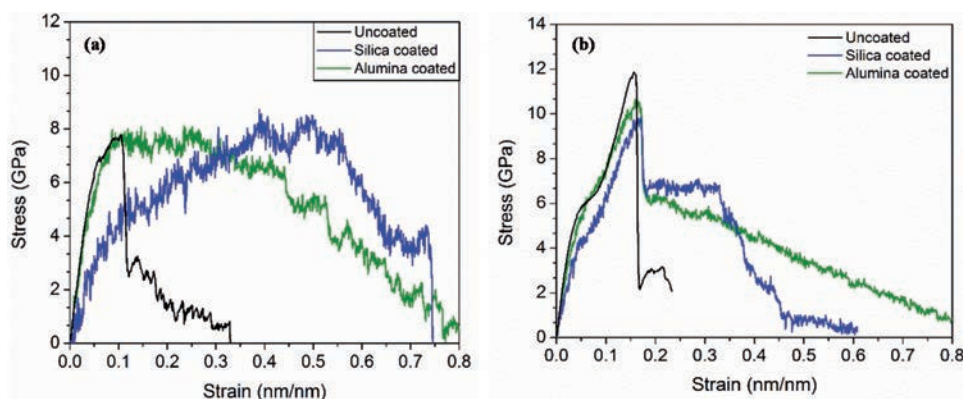


**Figure 4.** The effect of nanowire diameter is shown by comparing stress–strain curves for SiNWs (both coated and uncoated) with core diameter of a) 2 and b) 6 nm, with strain rate  $0.1\% \text{ ps}^{-1}$  at 300 K.

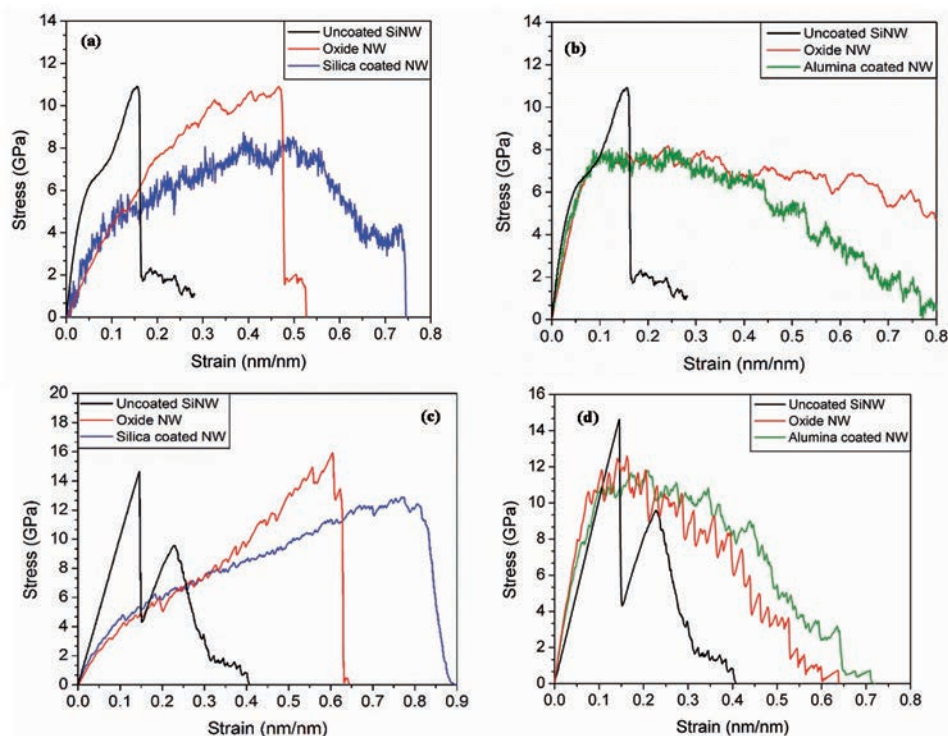


**Figure 5.** Stress–strain curves showing the effect of different coatings on the properties of SiNWs from a core–shell perspective: a) silica at 300 K, b) alumina at 300 K, c) silica at 0 K, and d) alumina at 0 K. In all cases, an SiNW and metal oxide nanowire of diameter 4 nm is compared to an SiNWs with a 2.0 nm core diameter and 1.0 nm thick coating.

not shown similar size dependence.<sup>[13]</sup> Therefore, it is expected that for the same coating thickness, as nanowire diameter increases the strain to failure should remain fairly constant for alumina-coated nanowires, but continue to decrease for silica-coated nanowires. This indicates that when coating thickness constraints exist for SiNWs with larger diameters, alumina coatings may be preferable, while silica coatings may be preferable at smaller diameters. Interestingly, silica-coated nanowires with 2 nm SiNW core diameters perform better in terms of ductility and toughness than nanowires made solely of either silicon or silica (Figure 5a). Although localized failure occurs in uncoated SiNWs at  $\approx 16\%$  strain, an SiNW with diameter of 2 nm and coating thickness of 1 nm displays uniform tensile elongation up to  $\approx 47\%$  strain, ultimately prolonging failure to 70% strain. Regardless, even a 1.0 nm thick coating continues to provide significant improvements in ductility and toughness for all diameters tested.

The increase in elongation to failure of the coated nanowires appears to be due to their ability to prevent localized failure from occurring (Figure 6a). In uncoated SiNWs, localized failure occurs as due to the formation of a dominant shear band, but both silica and alumina coatings delay the formation of shear band and can increase elongation to failure to 47% and greater. First, both silica- and alumina-coated nanowires are able to delay the formation of a dominant shear band by increasing the rate of defect nucleation.<sup>[48]</sup> Second, the strong electrochemical interactions between oxygen atoms in the coating and free surface bonds in the core silicon atoms distribute localized strains across a much greater volume and limit the flow

of core atoms within shear bands. This results in the formation of a relatively larger tensile neck and is likely the cause of the necking seen in experimental work of Han et al., found tensile necking in SiNWs with thin silica coatings.<sup>[42]</sup>

At 0 K, both silica and alumina coatings behave similarly to 300 K. While the uncoated SiNW was observed to fail upon neck formation, the coated SiNWs experienced prolonged necking that resulted in significantly increased elongation to failure. Consequently, although the uncoated SiNW possess the highest UTS of  $\approx 16$  GPa, energy absorbed to failure still increases significantly with coating. The effect of alumina coatings on the mechanical properties does not appear to change significantly between 0 and 300 K. However, the mechanical behavior of silica coatings is known to vary according to a number of parameters including temperature and strain rate.<sup>[49]</sup> At 0 K, the UTS and elongation to failure of silica increases significantly than at 300 K, increasing the ductility and toughness of silica-coated nanowires. This indicates that silica coatings may be preferable in lower temperature applications.

The dislocation mechanisms of the silicon nanowires show interesting properties under athermal conditions. As with the silica- and alumina-coated NWs at 300 K, and at 0 K, all the samples are able to increase ductility and toughness by impeding the formation of a tensile neck. In addition to careful examination of the Si core during deformation indicates twinning of the diamond cubic lattice via an intrinsic stacking fault on the glide set of {111} type planes (Figure 7). The mechanism of twinning for the Si diamond cubic structure involves the dissociation of full  $\langle 110 \rangle$  type dislocations into  $\langle 112 \rangle$  type Shockley partial

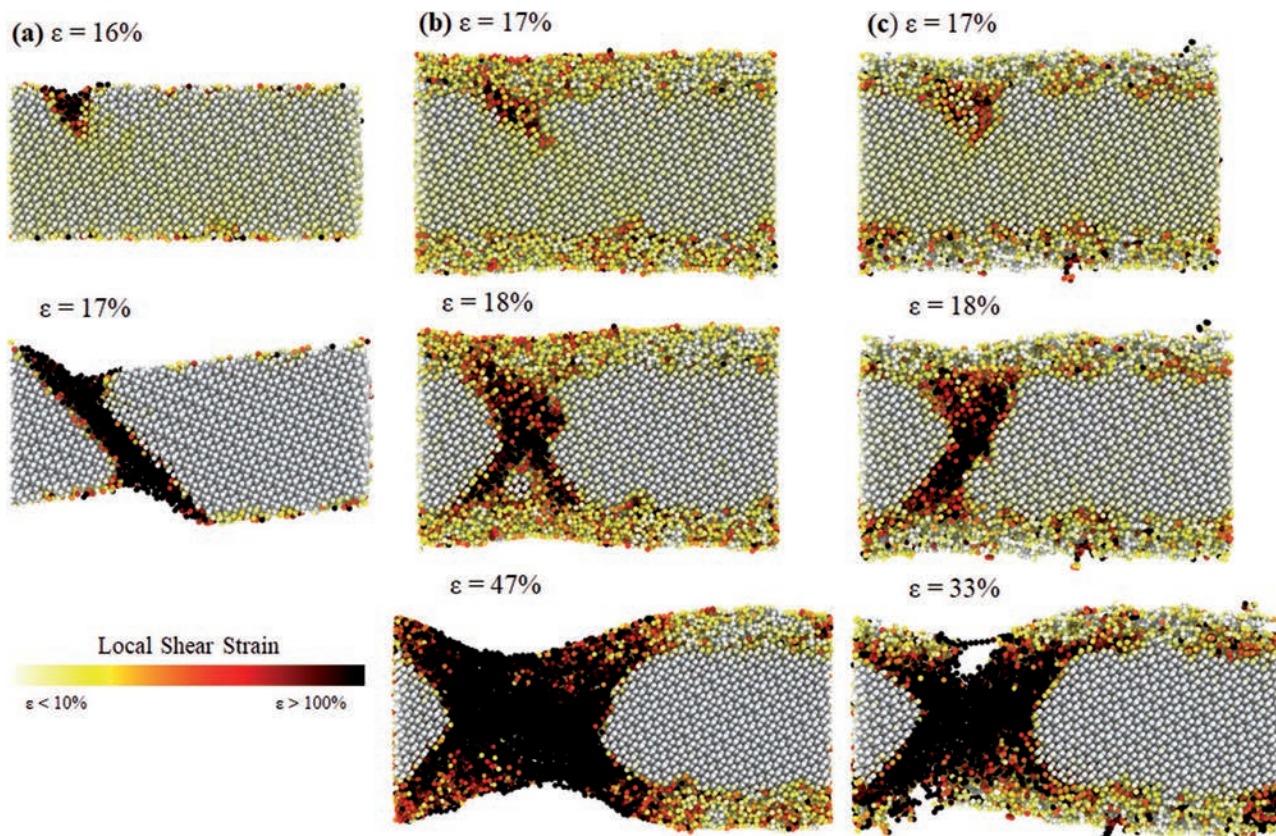


**Figure 6.** Snapshots comparing the failure mechanisms for SiNWs: a) uncoated, b) with 1.0 nm alumina coating, and c) with 1.0 nm silica coating at 300 K and with diameter of 6 nm. Atoms are colored according to the local shear strain invariant. A shear band is formed in all three nanowires between 16 and 17% strain, but although amorphization is highly localized in the uncoated SiNW, both coatings serve to distribute strain across a greater volume of material. In alumina coated nanowires, failure ultimately occurs after prolonged necking, while silica coated nanowires fail after fracture of the coating.

dislocations along the glide set. Since twinning leads to significant strain relaxation, this helps to permit sustained deformation of the core in the coated SiNWs. However, it should be noted that it is unclear to what extent these effects are due to reduced temperature or due to the lack of structural distortion at 0 K, resulting in different lattice properties between 0 and 300 K results. Dislocation-based plasticity has been previously observed in experimental studies of SiNWs, with full  $\langle 110 \rangle$  type dislocations being observed in tensile loadings of  $\langle 110 \rangle$  oriented wire samples. Although partial dislocation activity has not been directly observed in experimental studies of SiNWs, they appear readily in the growth of  $\langle 111 \rangle$  oriented SiNWs,<sup>[50]</sup> which suggests a low stacking fault energy and high tendency of formation for the partials.

### 3.3. Chemical Origins of Ductility Enhancement by Metal Oxide Coatings

In general, it is accepted that metal oxides are fairly brittle. Furthermore, previous simulations of oxidized iron and copper nanowires found that while the oxide coatings lowered the onset of plastic deformation, they failed to significantly improve overall ductility.<sup>[51,52]</sup> However, recently, Sen et al. showed that

oxidized aluminum nanowires are ductile and capable of superplastic deformation beyond 100% strain in an oxygen environment.<sup>[53]</sup> Interestingly, our results show that both alumina and silica coatings could improve the ductility of SiNWs even in vacuum. Silica, both by itself and as a coating material for SiNWs, quickly fractures when it approaches a strain of 47%. However, although the UTS of alumina occurs at 24% strain, it is able to prevent fracture until necking to much higher levels of strain, greater than 60%.

The large ductility of coated nanowires appears to be due to the ability of constituent atoms in the coating to undergo atomic rearrangement in response to strain. We estimate the number of overcoordinated atoms by using the first trough in the radial distribution function as a cutoff, with overcoordinated atoms having coordination above the median value. During tensile loading, strain energy is dissipated by the breaking of bonds between overcoordinated atoms, and voids are repaired as bonds form between undercoordinated atoms. However, as the number of overcoordinated atoms decreases, void growth occurs, increasing the number of undercoordinated atoms at the expense of over or normally coordinated atoms, as seen in the reduction in overcoordinated atoms in **Figure 8**. During tensile loading, the number of overcoordinated atoms in alumina decreases by  $\approx 12\%$ , allowing for a gradual decrease in the UTS

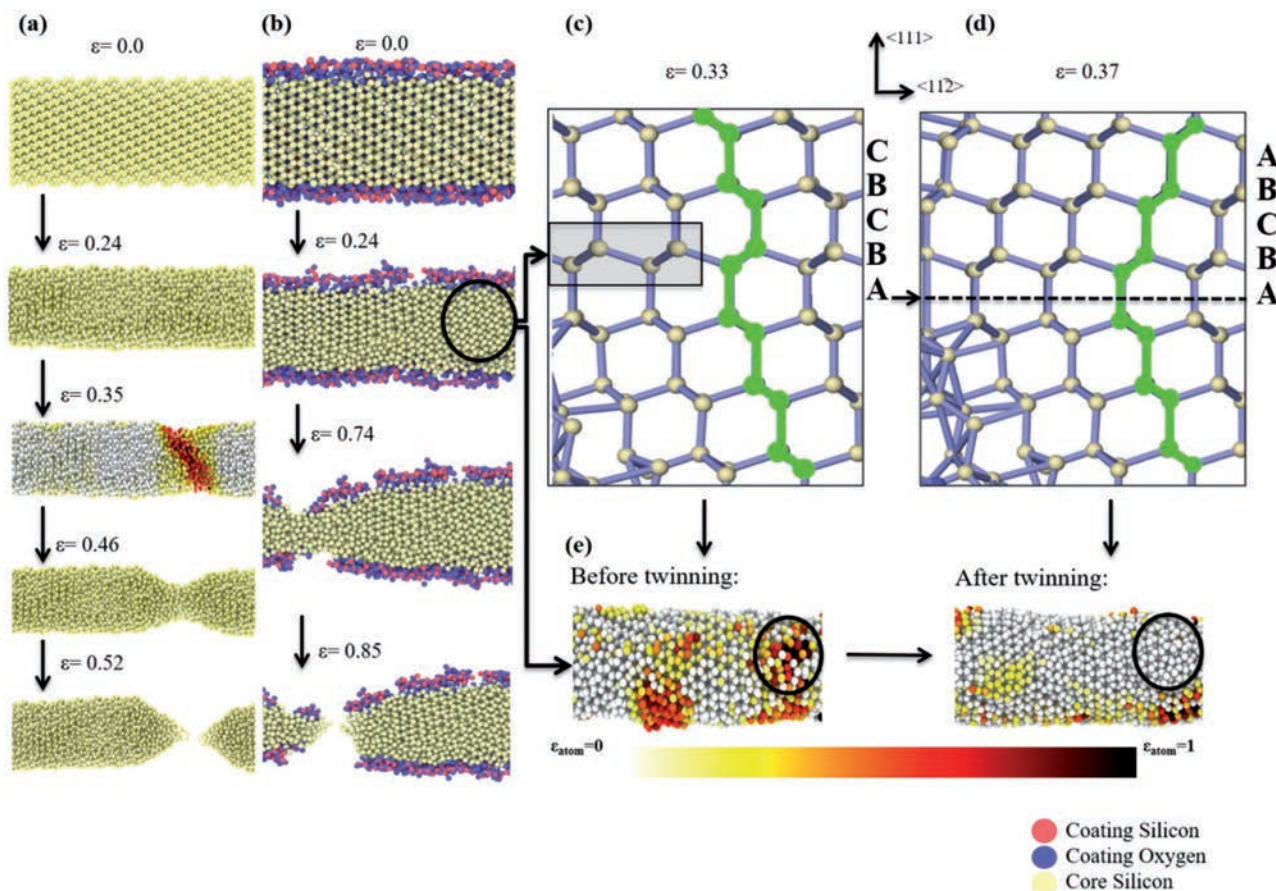


**Figure 7.** Snapshots showing stages that lead to fracture at 0 K and  $0.1\% \text{ ps}^{-1}$  in silicon nanowires at 0 K. For a) uncoated SiNWs, shear strain is localized in a single shear band prior to necking. In coated nanowires such as the pictured b) silica-coated SiNWs, c) the shaded region indicates the area of stacking fault that accompanies a  $30^\circ$  partial dislocation, and d) stacking faults that arise from twinning at  $\epsilon = 0.37$ . Both (c) and (d) also show formation of an amorphous region at the bottom right corner; e) higher strain experienced by each atom before twinning and lower strain after twinning. Atomic strain is expressed in the Lagrangian formulation as the local strain shear invariant.

of the alumina-coated nanowires via slow softening effect. This results in superior elongation to failure compared to silica coatings, which do not undergo significant atomic rearrangement and therefore fail quickly once a critical strain is reached. This

increased ductility is expected to be useful in designing coatings for Li-ion battery anodes, as ductile coating can limit exposure of the silicon core to the electrolyte even under significant strain to prevent SEI formation. However, it should be noted that nano-

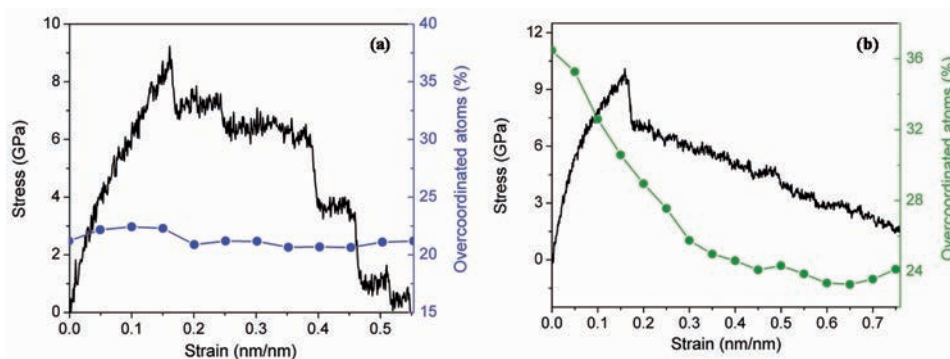


**Figure 8.** Graphs showing the percentage of overcoordinated atoms overlaid on the stress–strain curves for a) silica- and b) alumina-coated nanowires with core diameter of 4 nm and coating thickness of 1.0 nm. Silica coatings have a fewer proportion of overcoordinated atoms than alumina and are therefore less capable in absorbing strain energy through atomic rearrangement. The coordination number of an atom is estimated using the first trough in the radial distribution function as a cutoff, with overcoordinated atoms having coordination above the median value.

sized silica has also been found to be ductile when the average coordination number is high,<sup>[54,55]</sup> indicating this is not necessarily due to the cation species, but due to the higher atomic density in the alumina coating, which has greater than 50% more atoms in the same volume compared to the silica coating.

### 3.4. Application Toward Lithium-Ion Battery Anode Design

Our simulations have shown that the addition of metal oxide coatings results in significantly increased ductility and toughness, which is expected to improve long-term stability of SiNWs in Li-ion battery anodes where large volume expansion repeatedly occurs. Experimental results have shown that SiNWs with alumina and other metal oxide coatings have fewer cracks than uncoated nanowires following lithiation/delithiation.<sup>[13,14,19]</sup> Recently, Khosrownejad and Curtin<sup>[56]</sup> have found that fracture in lithiated SiNWs results due to the interaction of several processes including nanovoid nucleation and growth, localization of plastic flow between voids and the crack tip, and tearing of any residual ligaments. In our results, we found that failure in uncoated SiNWs occur via localized failure in a dominant shear band, but the addition of oxide coatings prevents localized failure from occurring due to strong interfacial bonding. In addition, it has been shown that silicon has significantly reduced yield stress when lithiated, with UTS decreasing from  $\approx 20$  GPa to less than 8 GPa in fully lithiated silicon,<sup>[57,58]</sup> but similar simulations on lithiated silica show a much lower decrease in yield stress.<sup>[27]</sup> Our simulations of metal oxide coated SiNWs show that the UTS of these systems follow mixing rules. As such, when the nanowire is lithiated, the slight decrease in UTS following the addition of the oxide coating may be less evident. These two factors are expected to significantly increase the toughness of the SiNW during lithiation/delithiation, preventing crack formation and fracture.

In addition, our simulations indicate that in order to be effective, the improvements in mechanical properties afforded by the metal oxide coatings should be relatively invariant of coating thickness. Although at a diameter size of 2 nm silica coatings perform reasonably well, with a toughness to failure of 4083 MJ, when the diameter size increases to 6 nm it falls to 2307 MJ. This is corroborated by experimental results, which show that although a 3.4 nm thick silica coating can improve the mechanical properties of SiNWs with a diameter of  $\approx 50$  nm, its effect becomes negligible when the diameter increases to 150 nm.<sup>[46,47]</sup> As coating thicknesses increases, electrochemical performance is expected to be negatively affected, as the need to repeatedly break Li–O bonds in the oxide coating presents a barrier to lithium diffusion.<sup>[27]</sup> Our results indicate that this problem can be mitigated by choosing metal oxide coatings which are sufficiently dense and results in relatively size invariant ductility due to the ability to undergo atomic rearrangement in response to strain. This allows for a mechanically robust coating which is nevertheless thin enough so as to not interfere with electrochemical performance.

Finally, it should be noted that although metal oxide coatings greatly improve the cycling stability of SiNWs as LIB anodes, reduction in charge capacity still occurs following 50–100 cycles due to breakup of the metal oxide coating.<sup>[13,14]</sup> As such, further

research is required in order to develop anode shapes and coating materials, taking into account both mechanical and electrochemical properties, and incorporating variables such as the presence of SEI layer and repeated lithiation/delithiation cycling.

## 4. Conclusion

The mechanical properties of uncoated, silica-coated, and alumina-coated SiNWs under uniaxial tensile loading were examined using classical MD simulations. The effects of parameters such as temperature, core diameter, and coating thickness were varied in order to study their effect on the mechanical response of the SiNWs. Our results revealed almost twofold gains in the ductility of the coated SiNWs, with increases in elongation-to-failure from 16% to greater than 47%. Importantly, the improvements in the ductility of nanowires were not accompanied by a proportional decrease in the tensile strength, resulting in remarkable improvements in toughness of up to  $\approx 4$  times. The oxide coatings dissipate strain energy via atomic rearrangement of overcoordinated atoms, an effect most notable when the oxide coating is highly coordinated while also increasing the activation volume of the silicon core, preventing localized deformation from occurring. This increase in toughness and ductility is therefore expected to improve long-term stability of SiNWs in Li-ion battery anodes and other energy storage and electronics applications.

## Supporting Information

Supporting Information is available from the Wiley Online Library or from the author.

## Acknowledgements

The authors acknowledge funding by the Natural Sciences and Engineering Research Council of Canada (NSERC) through the Discovery grant, and undergraduate and postgraduate scholarship programs, the Hart Professorship, and the University of Toronto. The authors would also like to thank Alexander Stukowski (TU Darmstadt) for his kind guidance concerning the use of OVITO. The authors also acknowledge Compute Canada for providing computing resources at the SciNet Calcul Quebec, and Westgrid consortia. The authors also thank Hao Sun and Gurjot Dhaliwal for important discussions.

## Conflict of Interest

The authors declare no conflict of interest.

## Keywords

ductility, Li-ion batteries, molecular dynamics, oxide coatings, silicon nanowires

Received: July 30, 2017  
Revised: August 21, 2017  
Published online:

- [1] W. Lu, C. M. Lieber, *J. Phys. D* **2006**, *387*, R387.
- [2] J. Izuan, A. Rashid, J. Abdullah, N. A. Yusof, R. Hajian, *J. Nano-mater.* **2013**, *2013*, 328093.
- [3] F. Liao, T. Wang, M. Shao, *J. Mater. Sci.* **2015**, *26*, 4722.
- [4] C. K. Chan, H. Peng, G. Liu, K. McIlwrath, X. F. Zhang, R. A. Huggins, Y. Cui, *Nat. Nanotechnol.* **2008**, *3*, 31.
- [5] M. N. Obrovac, V. L. Chevrier, *Chem. Rev.* **2014**, *114*, 11444.
- [6] P. Meister, H. Jia, J. Li, R. Kloepsch, M. Winter, T. Placke, *Chem. Mater.* **2016**, *28*, 7203.
- [7] U. Kasavajjula, C. Wang, A. J. Appleby, *J. Power Sources* **2007**, *163*, 1003.
- [8] X. H. Liu, L. Zhong, S. Huang, S. X. Mao, T. Zhu, J. Y. Huang, *ACS Nano* **2012**, *6*, 1522.
- [9] C. Pereira-Nabais, J. wiatowska, A. Chagnes, A. Gohier, S. Zanna, A. Seyeux, P. Tran-Van, C. S. Cojocar, M. Cassir, P. Marcus, *J. Phys. Chem. C* **2014**, *118*, 2919.
- [10] T. Song, J. L. Xia, J.-H. Lee, D. H. Lee, M.-S. Kwon, J.-M. Choi, J. Wu, S. K. Doo, H. Chang, W. I. Park, D. S. Zang, H. Kim, Y. G. Huang, K.-C. Hwang, J. A. Rogers, U. Paik, *Nano Lett.* **2010**, *10*, 1710.
- [11] R. Huang, X. Fan, W. Shen, J. Zhu, *Appl. Phys. Lett.* **2009**, *95*, 133119.
- [12] Y. Yao, N. Liu, M. T. McDowell, M. Pasta, Y. Cui, *Energy Environ. Sci.* **2012**, *5*, 7927.
- [13] H. T. Nguyen, M. R. Zamfir, L. D. Duong, Y. H. Lee, P. Bondavalli, D. Pribat, *J. Mater. Chem.* **2012**, *22*, 24618.
- [14] E. Memarzadeh Lotfabad, P. Kalisvaart, K. Cui, A. Kohandehghan, M. Kupsta, B. Olsen, D. Mitlin, *Phys. Chem. Chem. Phys.* **2013**, *15*, 13646.
- [15] X. Meng, X.-Q. Yang, X. Sun, *Adv. Mater.* **2012**, *24*, 3589.
- [16] P. Katiyar, C. Jin, R. J. Narayan, *Acta Mater.* **2005**, *53*, 2617.
- [17] K. Leung, Y. Qi, K. R. Zavadil, Y. S. Jung, A. C. Dillon, A. S. Cavanagh, S. Lee, S. M. George, *J. Am. Chem. Soc.* **2011**, *133*, 14741.
- [18] C. K. Chan, R. Ruffo, S. Sae, Y. Cui, *J. Power Sources* **2009**, *189*, 1132.
- [19] S. Kim, A. Ostadhossein, A. C. T. van Duin, X. Xiao, H. Gao, Y. Qi, *Phys. Chem. Chem. Phys.* **2016**, *18*, 3706.
- [20] Y. He, X. Yu, Y. Wang, H. Li, X. Huang, *Adv. Mater.* **2011**, *23*, 4938.
- [21] Y. He, H. Hu, K. Zhang, S. Li, J. Chen, *J. Mater. Sci.* **2017**, *52*, 2836.
- [22] A. C. T. van Duin, S. Dasgupta, F. Lorant, W. A. Goddard, *J. Phys. Chem. A* **2001**, *105*, 9396.
- [23] B. Narayanan, A. C. T. van Duin, B. B. Kappes, I. E. Reimanis, C. V. Ciobanu, *Modell. Simul. Mater. Sci. Eng.* **2012**, *20*, 15002.
- [24] J. Guérolé, J. Godet, S. Brochard, J. Gu, *Phys. Rev. B* **2013**, *87*, 1.
- [25] J. Godet, C. Furgeaud, L. Pizzagalli, M. J. Demkowicz, *Extrem. Mech. Lett.* **2016**, *8*, 151.
- [26] S. Plimpton, *J. Comput. Phys.* **1995**, *117*, 1.
- [27] A. Ostadhossein, S. Y. Kim, E. D. Cubuk, Y. Qi, A. C. T. Van Duin, *J. Phys. Chem. A* **2016**, *120*, 2114.
- [28] U. Khalilov, G. Pourtois, A. Bogaerts, A. C. T. van Duin, E. C. Neyts, *Nanoscale* **2013**, *5*, 719.
- [29] B. Ding, H. Wu, Z. Xu, X. Li, H. Gao, *Nano Energy* **2017**, *38*, 486.
- [30] S. Nose, *J. Chem. Phys.* **1984**, *81*, 511.
- [31] A. Stukowski, *Modell. Simul. Mater. Sci. Eng.* **2010**, *18*, 015012.
- [32] A. Stukowski, *Modell. Simul. Mater. Sci. Eng.* **2012**, *20*, 045021.
- [33] W. Liu, K. Zhang, H. Xiao, L. Meng, *Nanotechnology* **2007**, *18*, 215703.
- [34] E. Maras, O. Trushin, A. Stukowski, T. Ala-Nissila, H. Jonsson, *Comput. Phys. Commun.* **2016**, *205*, 13.
- [35] H. Zhang, J. Tersoff, S. Xu, H. Chen, Q. Zhang, K. Zhang, Y. Yang, C. Lee, K. Tu, J. Li, Y. Lu, *Sci. Adv.* **2016**, *2*, 1.
- [36] K. Kang, W. Cai, P. Taylor, K. Kang, W. Cai, *Philos. Mag.* **2007**, *87*, 2169.
- [37] K. Kang, W. Cai, *Int. J. Plast.* **2010**, *26*, 1387.
- [38] Z. Yang, Z. Lu, Y. Zhao, *J. Appl. Phys.* **2009**, *106*, 23537.
- [39] J. Guérolé, J. Godet, S. Brochard, *Modell. Simul. Mater. Sci. Eng.* **2011**, *19*, 74003.
- [40] D.-M. Tang, C.-L. Ren, M.-S. Wang, X. Wei, N. Kawamoto, C. Liu, Y. Bando, M. Mitome, N. Fukata, D. Golberg, *Nano Lett.* **2012**, *12*, 1898.
- [41] Q. Liu, S. Shen, *Int. J. Plast.* **2012**, *38*, 146.
- [42] X. D. D. Han, K. Zheng, Y. F. F. Zhang, X. N. N. Zhang, Z. Zhang, Z. L. L. Wang, *Adv. Mater.* **2007**, *19*, 2112.
- [43] Y. He, L. Zhong, F. Fan, C. Wang, T. Zhu, S. X. Mao, *Nat. Nano-technol.* **2016**, *11*, 866.
- [44] Y. Wang, W. Zhang, L. Wang, Z. Zhuang, E. Ma, J. Li, Z. Shan, *NPG Asia Mater.* **2016**, *8*, e291.
- [45] S. Zhang, *npj Comput. Mater.* **2017**, *3*, 1.
- [46] S. Sim, P. Oh, S. Park, J. Cho, *Adv. Mater.* **2013**, *25*, 1.
- [47] M. T. McDowell, S. W. Lee, I. Ryu, H. Wu, W. D. Nix, J. W. Choi, Y. Cui, *Nano Lett.* **2011**, *11*, 4018.
- [48] T. Zhu, J. Li, A. Samanta, H. G. Kim, S. Suresh, *Proc. Natl. Acad. Sci. USA* **2007**, *104*, 3031.
- [49] S. Chowdhury, B. Z. Haque, J. W. Gillespie Jr., *J. Mater. Sci.* **2016**, *51*, 10139.
- [50] J. Arbiol, S. Estradé, F. Peiró, B. Kalache, P. Roca, J. R. Morante, *J. Appl. Phys.* **2008**, *104*, 64312.
- [51] M. D. Skarlinski, D. J. Quesnel, M. D. Skarlinski, D. J. Quesnel, *J. Appl. Phys.* **2015**, *118*, 235306.
- [52] G. Aral, Y. Wang, S. Ogata, A. C. T. Van Duin, *J. Appl. Phys.* **2016**, *120*, 135104.
- [53] F. G. Sen, A. T. Alpas, A. C. T. van Duin, Y. Qi, *Nat. Commun.* **2014**, *5*, 3959.
- [54] F. Yuan, L. Huang, *Sci. Rep.* **2014**, *4*, 5035.
- [55] Y. Xu, M. Wang, N. Hu, C. Yan, *RSC Adv.* **2016**, *6*, 28121.
- [56] S. M. Khosrownejad, W. A. Curtin, *J. Mech. Phys. Solids* **2017**, *107*, 542.
- [57] J. L. Akihiro Kushima, J. Y. Huang, *ACS Nano* **2012**, *6*, 9425.
- [58] F. Fan, S. Huang, H. Yang, M. Raju, *Modell. Simul. Mater. Sci. Eng.* **2013**, *21*, 74002.